

Inverse analysis of metamaterials and parameter determination by means of an automatized optimization problem

Navid Shekarchizadeh¹  | Bilen Emek Abali^{2,3}  | Emilio Barchiesi⁴  | Alberto Maria Bersani⁵ 

¹ Department of Basic and Applied Sciences for Engineering, Sapienza University of Rome, Via Antonio Scarpa, 16, Rome 00161, Italy

² Institute of Mechanics, Technische Universität Berlin, Einsteinufer 5, Berlin 10967, Germany

³ Division of Applied Mechanics, Uppsala University, Department of Materials Science and Engineering, Box 534, Uppsala 751 21, Sweden

⁴ International Research Center on Mathematics and Mechanics of Complex Systems, Università degli Studi dell'Aquila, Via Giovanni Gronchi 18 - Zona industriale di Pile, L'Aquila 67100, Italy

⁵ Department of Mechanical and Aerospace Engineering, Sapienza University of Rome, Via Eudossiana 18, Rome 00184, Italy

Correspondence

Bilen Emek Abali, Institute of Mechanics, Technische Universität Berlin, Einsteinufer 5, 10967 Berlin, Germany.
Email: bilenemek@abali.org

In this paper, a novel parameter determination technique is developed for material models in continuum mechanics aimed at describing metamaterials. Owing to their peculiar mechanical properties and behaviors, such as extreme elasticity or high strength-to-weight ratio, metamaterials are of interest to be simulated by reduced-order modeling by means of the generalized mechanics. Such models incorporate constitutive parameters to be determined; we develop an automatized optimization process specifically for obtaining metamaterials parameters. The process aims at minimizing a mechanically meaningful error function measuring the deviation of the continuum from a detailed description by using the Trust Region Reflective optimization method. The parameter identification procedure is tested for an exemplary extension experiment of a metamaterial, proving to be robust and reliable.

KEYWORDS

Finite Element Method (FEM), inverse analysis, metamaterials, optimization

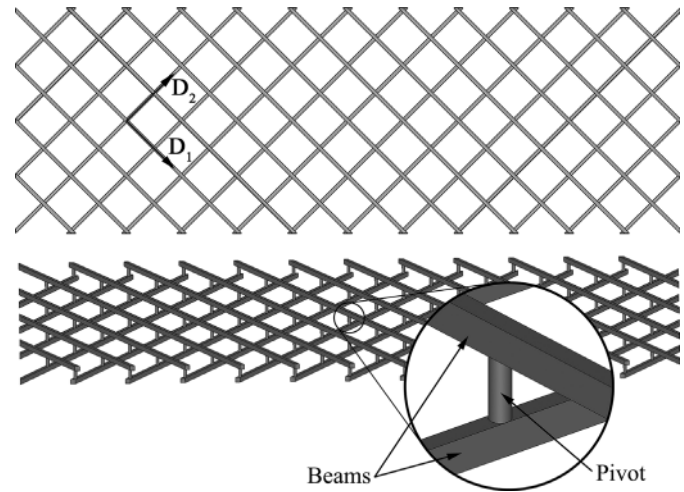
1 | INTRODUCTION

The design and construction of structures with peculiar mechanical properties are of paramount interest. The design and topology optimization of structures possessing high toughness such as composite materials [1–4] has been widely studied. Metamaterials are the family of materials that are architected with tailored material properties by using an optimized topology with an inner substructure. Pantographic lattice, as a macro-scale example of metamaterials, is a structure consisting of two groups of parallel equispaced beams (fibers) which are connected to each other by cylindrical pivots at their intersections. The two groups of fibers are orthogonal in the initial frame [5] (see Figure 1). These days, samples of this structure are produced by virtue of 3D printing technology [6].

This is an open access article under the terms of the [Creative Commons Attribution](https://creativecommons.org/licenses/by/4.0/) License, which permits use, distribution and reproduction in any medium, provided the original work is properly cited.

© 2021 The Authors. *ZAMM - Journal of Applied Mathematics and Mechanics* published by Wiley-VCH GmbH.

FIGURE 1 A CAD model of a pantographic structure created in SALOME



For describing the pantographic structures, it is possible to employ the Cauchy continuum theory. For a short history of the mechanics theory, see [7]. In this paper, “micro-scale” does not correspond to any specific length-scale but rather it means that at one (or more) smaller length-scale(s) than “macro-scale” (at which the phenomena are perceived by the naked eye), the material is comprised of complex substructures.

In the Cauchy continuum theory, the immediate neighborhood of a particle is described by the first derivative in space. This neighborhood is an infinitesimally small spherical region. In numerical mechanics, the radius of this region should be set to a value smaller than the length-scale of the structure. This makes the analysis of the pantographic lattice computationally costly since it has a micro-scale underlying structure, i.e., the pantographic structure has a micro-scale length-scale. An efficient solution method is using generalized continuum mechanics [8], i.e., including second or higher gradients of displacement in the model, and thus, having additional material parameters than the classical theories [9, 10]. In this approach, we do not need to consider the detailed geometry of the structure. Instead, a homogenized model is developed [11]. In this way, the length-scale will become relatively large. The effect of the microstructure is captured through the new coefficients added to the model [12, 13]. In the end, we have a reduced-order homogenized model that is solved fast, numerically as in [14].

Theories considering the higher gradients of the displacement are applied, for example, to elasticity [15–18], to inelastic models [19], to plasticity [20–23], to anisotropic elasticity [24], to thermo-elasto-plasticity [25], for dissipative systems [26], to wave propagation analysis [27], to gradient-enhanced homogenization [28, 29], using asymptotic analysis [30], to micromorphic continuum [31], to the Kirchhoff plates [32, 33], to the Timoshenko beam [34], and to bone remodeling [35].

Many reduced-order continuum models for describing the pantographic structures have been presented in the literature, such as those assuming inextensible fibers [36–40] or using discrete [41–45], semi-discrete [46–48], and continuum models [49–53], and the meso- to macro-scale homogenization models [42, 54, 55], see [56, 57] for a review. The bending of pantographic structures has been investigated numerically and experimentally in [58, 59]. Through a homogenization procedure [60], the behavior of the structure is estimated by the reduced-order model [61, 62]. The existence and uniqueness of weak solutions for linear pantographic structures is presented in [63, 64]. The wave dispersion in nonlinear pantographic beams has been studied [65]. The dynamical behavior of a pantographic sheet is investigated experimentally in [66, 67]. In [68], the compression of polyamide pantographic fabrics is studied. A so-called bi-pantographic fabric is investigated in [69]. A discrete model is used for the homogenization of the large in-plane elastic deformation of the bi-pantographic structure, and the results are validated experimentally. For homogenization of pantographic structures possessing flexoelectric and piezoelectric properties see [70, 71].

In [72], a predictive macro model is presented for characterizing large displacements and large deformations in planar pantographic structures assuming extensible beams. This continuum model is based on a meso-scale to macro-scale homogenization technique for formulating a fully nonlinear beam model that is developed based on a discrete system of extensional and rotational springs and masses. The considered energy expression depends on second-gradient displacement terms. In an improved model [73], the pantographic structure is described in a two-dimensional formulation embedded in three-dimensional space. The model takes account of large out-of-plane motions. There are second space derivatives of the displacement in the deformation energy formulation for considering the in-plane and out-of-plane bending and twisting of fibers. In [74], a numerical identification is performed to fit the parameters of the macro model of planar pantographic structures, where the total stored strain energy and two angles in the structure are considered. It is

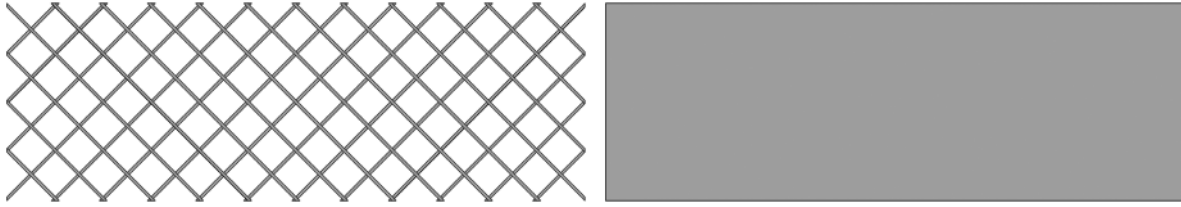


FIGURE 2 Left: micro-scale model with the detailed information of the substructure leading to a high computational cost. Right: macro-scale model, i.e., metamaterial representing the same mechanical response of the micro-scale one by using the generalized mechanics leading to a reduced-order modeling with a low computational cost

shown that the reduced-order method is able to model the structure accurately with a significantly lower computational cost. In [75], through an inverse analysis, the material parameters in the elastic energy description of the aforementioned improved model are determined. The in-plane and out-of-plane stiffnesses are determined by simulating bias extension and shear tests and employing the Levenberg–Marquardt optimization algorithm. In [76], the numerical identification of the constitutive parameters of the aforementioned predictive macro model is carried out through genetic algorithm [77] and Nondominated Sorting Genetic Algorithm II (NSGA-II) [78] optimization methods. Considering the above-mentioned literature, developing an automatized optimization process for identifying the constitutive parameters of metamaterials is the main objective of the underlying work.

In this research, we aim at implementing the conventional elasticity theory on a pantographic structure, and solve it numerically by following the computational methods by means of the finite element method (FEM) as in [79]. Then a macro-scale homogenized model is employed for modeling the structure at a reduced computational cost. The parameters of the macro-scale model are identified through an automatized optimization process, and the reliability of the model is assessed.

The paper is organized in the following way: in Section 2, we briefly explain the micro-scale nonlinear elastostatic model in continuum mechanics and a second-gradient macro-scale model. In Section 3, we identify the parameters of the macro-scale model through an optimization problem. To this aim, a fully automatized optimization problem is developed and implemented in the Python language. In Section 4, the micro-scale and macro-scale models of a pantographic structure are implemented for obtaining the deformation in the structure. In Section 5, we present the results of the simulation of a tensile test on the pantographic structure obtained from micro- and macro-scale models. Also, the results of the parameter determination process are given. In Section 6, the conclusions and perspectives are discussed.

2 | CONTINUUM MECHANICS MODELS

In this section, the micro-scale nonlinear elastostatic model in continuum mechanics and a second-gradient macro-scale model are briefly explained. Consider the micro-scale model with the substructure and its corresponding homogenized model as demonstrated in Figure 2.

2.1 | Micro-scale model

In the Lagrangean frame, we assume that a continuum body initially occupying $\mathcal{B}_0 \subset \mathbf{R}^3$ deforms to the current frame occupying $\mathcal{B} \subset \mathbf{R}^3$, expressed in Cartesian coordinates. The position of the particles at the initial time, t_0 , is identified by \mathbf{X} and they move to \mathbf{x} at the current time, t , by undergoing the displacement $\mathbf{u}(\mathbf{X}, t)$. Therefore, we have

$$x_i = X_i + u_i. \quad (1)$$

By defining the deformation gradient as $F_{ij} = \frac{\partial x_i}{\partial X_j}$, the Green–Lagrange strain tensor is defined as

$$\begin{aligned} E_{ij} &= \frac{1}{2}(F_{ki}F_{kj} - \delta_{ij}) \\ &= \frac{1}{2}(u_{k,i}u_{k,j} + u_{i,j} + u_{j,i}), \end{aligned} \quad (2)$$

where we use the Einstein summation convention over repeated indices, comma denotes a partial derivative with respect to \mathbf{X} in the Lagrangean frame and δ_{ij} is the Kronecker delta, which denotes an identity matrix. As the strain measure is nonlinear, the model is valid for large deformations such that it is capable of capturing geometrical nonlinearities.

The density of stored energy, W_m , is defined as a function of the Green–Lagrange strain tensor and the Lamé parameters of the material, λ, μ , as

$$W_m(\mathbf{E}) = \frac{\lambda}{2} E_{kk}^2 + \mu E_{ij} E_{ij}. \quad (3)$$

Here, for obtaining the governing equations of the structure, we exploit the formulation based on action principles [80]. An action like energy is used as

$$\mathcal{A} = \int_{B_0} \left(\frac{1}{2} \rho_0 \dot{u}_i \dot{u}_i - W_m + \rho_0 f_i u_i \right) dV + \int_{\partial B_0^N} \hat{t}_i u_i dA, \quad (4)$$

where the primitive variable is the displacement u_i . In Equation (4), the first term accounts for the kinetic energy where ρ_0 and \dot{u}_i are the mass density at the initial frame and the time derivative of displacement, respectively. The third term, $\rho_0 f_i u_i$, is the potential energy density (per volume) and f_i is the specific (per mass) gravitational force. The second integral is for the work done on the surfaces where \hat{t}_i is the traction vector applied on the Neumann boundary ∂B_0^N .

In quasi-static conditions, the continuum body deforms slowly such that the inertial terms are negligible. If the deformation caused by the mass of the body compared to the deformation due to applied force is negligible, the force term can also be ignored. According to the *principle of least action*, for arbitrary values of the test function δu , the variation of the action like the functional in Equation (4) vanishes, as follows:

$$\delta \mathcal{A} = 0 \quad \forall \delta u. \quad (5)$$

Employing the variational formulation leads to the weak form of the micro-scale model as below:

$$- \int_{B_0} \frac{\partial W_m}{\partial u_{i,j}} \delta u_{i,j} dV + \int_{\partial B_0^N} \hat{t}_i \delta u_i dA = 0, \quad (6)$$

where we apply the chain rule for computation of the first term as

$$\frac{\partial W_m}{\partial u_{i,j}} = \frac{\partial W_m}{\partial E_{kl}} \frac{\partial E_{kl}}{\partial u_{i,j}}. \quad (7)$$

By solving the weak form of Equation (6) numerically, the displacement u_i is obtained for the whole body.

2.2 | Macro-scale model

For characterizing the behavior of planar pantographic structures, the reduced-order model of [72] is employed here. In this model, a homogenization from meso-scale to macro-scale is carried out. In the formulation of this homogenized model, the stretching and bending stiffnesses of the fibers, as well as the shear stiffness of the cylindrical connecting pivots, are considered. The model is briefly explained in the following.

The placement χ maps a material point from \mathbf{X} in the initial frame to \mathbf{x} in the current frame through the displacement \mathbf{u} . In the map $\chi : \Omega \rightarrow \mathbf{R}^2$, Ω is chosen as a rectangular plane region. A Cartesian orthogonal coordinate system, with the unit base vectors of $(\mathbf{D}_1, \mathbf{D}_2)$, is assumed to be aligned in the direction of the two families of fibers (see Figure 1).

$$\mathbf{x} = \begin{pmatrix} x_1 \\ x_2 \end{pmatrix} = \chi(X_1, X_2) = (X_1 + u_1(\mathbf{X}))\mathbf{D}_1 + (X_2 + u_2(\mathbf{X}))\mathbf{D}_2 \quad (8)$$

The deformation gradient is $\nabla\chi$ and the vectors \mathbf{e}_1 and \mathbf{e}_2 show the orientation of the fibers after deformation (in the current frame),

$$\nabla\chi = \begin{bmatrix} \frac{\partial x_1}{\partial X_1} & \frac{\partial x_1}{\partial X_2} \\ \frac{\partial x_2}{\partial X_1} & \frac{\partial x_2}{\partial X_2} \end{bmatrix}, \quad (9)$$

$$\mathbf{e}_1 = \frac{(\nabla\chi)\mathbf{D}_1}{\|(\nabla\chi)\mathbf{D}_1\|} \quad \text{and} \quad \mathbf{e}_2 = \frac{(\nabla\chi)\mathbf{D}_2}{\|(\nabla\chi)\mathbf{D}_2\|}, \quad (10)$$

where $\|\cdot\|$ means the L_2 norm. In this model, the ‘‘stretch of fibers’’ and the ‘‘fiber geodesic curvature’’ are defined by $\boldsymbol{\varepsilon}$ and $\boldsymbol{\kappa}$, respectively,

$$\boldsymbol{\varepsilon} = \begin{pmatrix} \varepsilon_1 \\ \varepsilon_2 \end{pmatrix} = \begin{pmatrix} \|(\nabla\chi)\mathbf{D}_1\| - 1 \\ \|(\nabla\chi)\mathbf{D}_2\| - 1 \end{pmatrix}, \quad (11)$$

$$\boldsymbol{\kappa} = \begin{pmatrix} \kappa_1 \\ \kappa_2 \end{pmatrix} = \begin{pmatrix} \|\mathbf{c}_1 - (\mathbf{c}_1 \cdot \mathbf{e}_1)\mathbf{e}_1\| \\ \|\mathbf{c}_2 - (\mathbf{c}_2 \cdot \mathbf{e}_2)\mathbf{e}_2\| \end{pmatrix}, \quad (12)$$

where,

$$\mathbf{c}_1 = \frac{\begin{pmatrix} \frac{\partial^2 \chi_1}{\partial X_1^2} \\ \frac{\partial^2 \chi_2}{\partial X_1^2} \end{pmatrix}}{\|(\nabla\chi)\mathbf{D}_1\|} \quad \text{and} \quad \mathbf{c}_2 = \frac{\begin{pmatrix} \frac{\partial^2 \chi_1}{\partial X_2^2} \\ \frac{\partial^2 \chi_2}{\partial X_2^2} \end{pmatrix}}{\|(\nabla\chi)\mathbf{D}_2\|}. \quad (13)$$

The vectors \mathbf{c}_1 and \mathbf{c}_2 contain second-gradient terms of displacement, which are incorporated in the stored energy definition by means of the generalized continuum. This second-order theory is a subset of the strain gradient theory, since $\boldsymbol{\kappa}$ contains the second-gradient of χ which is the gradient of the strain $\boldsymbol{\varepsilon}$. The shear distortion, γ , is the change of the angle between two specific fibers from two families of initially orthogonal fibers, defined as

$$\gamma = \arcsin(\mathbf{e}_1 \cdot \mathbf{e}_2). \quad (14)$$

The strain energy density of the macro-scale model, W_M , is defined as

$$W_M(\boldsymbol{\varepsilon}, \boldsymbol{\kappa}, \gamma) = \frac{1}{2}K_e(\varepsilon_1^2 + \varepsilon_2^2) + \frac{1}{2}K_g(\kappa_1^2 + \kappa_2^2) + \frac{1}{2}K_s\gamma^2. \quad (15)$$

The strain energy density consists of the energy terms of elongation and geodesic bending of the fibers and the torsion of the connecting pivots. The K_e, K_g, K_s are the stretching, geodesic bending, and the shear stiffnesses, respectively, which are positive and constant constitutive parameters of the macro-scale model. The geodesic bending is the bending that occurs in a fixed plane and it has strain-gradient effects in the continuum theory [81].

Here, analogous to the previous section, we utilize the action principles by utilizing the energy density of the macro-scale model in Eq. (15). Based on the principle of least action in Eq. (5), the weak form for macro-scale model is obtained as

$$-\int_{B_0} \frac{\partial W_M(\boldsymbol{\varepsilon}, \boldsymbol{\kappa}, \gamma)}{\partial u_{i,j}} \delta u_{i,j} dV + \int_{\partial B_0^N} \hat{i}_i \delta u_i dA = 0, \quad (16)$$

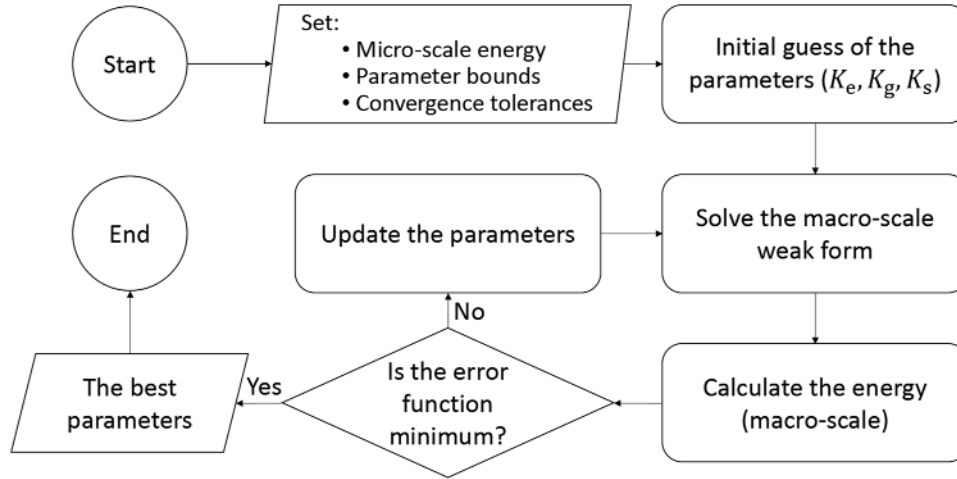


FIGURE 3 The flowchart of the numerical identification process

where

$$\frac{\partial W_M(\boldsymbol{\varepsilon}, \boldsymbol{\kappa}, \gamma)}{\partial u_{i,j}} = \frac{\partial W_M}{\partial \varepsilon_k} \frac{\partial \varepsilon_k}{\partial u_{i,j}} + \frac{\partial W_M}{\partial \kappa_k} \frac{\partial \kappa_k}{\partial u_{i,j}} + \frac{\partial W_M}{\partial \gamma} \frac{\partial \gamma}{\partial u_{i,j}}. \quad (17)$$

3 | OPTIMIZATION

The goal of the optimization problem is to identify the parameters of the macro-scale model by fitting its results with the micro-scale model. In the following, the details of the numerical identification process and the optimization algorithm are discussed.

3.1 | Numerical identification

The identification of the parameters of the macro-scale model (K_e , K_g , and K_s in Equation (15)) is done numerically through an optimization problem. The optimization procedure minimizes an error measure yet to be defined. The least restrictive hypothesis is that the micro-scale and macro-scale models have the same deformation energy. However, we emphasize that the displacements in both scales are different, as well as the local deformation energy density, although the total deformation energy is the same, applied by the same work done on boundaries. In a well-posed problem, the boundaries are given such that we expect that the same energy over the boundaries is transferred to the macro-scale model as well as to the micro-scale model. By the total deformation (or stored) energy, we mean the deformation energy stored in the whole structure. We use the energy difference between the micro- and macro-scale models as the error measure for optimization; any other additional measure like matching boundaries or the same curvature could be introduced by Lagrange multipliers [82].

3.2 | Optimization algorithm

We automatize an optimization problem for determining metamaterials parameters, and implement it in the Python language. We have made use of the *optimization* submodule of the *Scipy* package [83]. A flowchart of the optimization process and the numerical identification is shown in Figure 3. In this process, at first, the micro-scale energy, bounds of the parameters, and the convergence tolerances are set as input parameters. Then, for the first iteration of the optimization, we need an initial guess of the parameters for calculating the macro-scale energy. In every iteration, the parameters are updated, until at least one of the convergence criteria stops the iteration, and the solution is the output.

TABLE 1 Geometrical parameters used for constructing the geometry as suggested in [46], the formula for the initial guess of the parameters as suggested in [75], and the parameters determined the optimization problem

Geometrical Parameters (mm)						
L	l	h_b	w_b	p_b	h_p	d_p
210	70	1.6	1	12.15	3	1
Constitutive Parameters						
Parameter	Initial Guess			Final Results		
K_e (N/m)	$K_e^0 = \frac{Ew_b h_b}{p_b} = 2.107 \times 10^5$			1.406×10^5		
K_g (Nm)	$K_g^0 = \frac{EI_z}{p_b} = 1.756 \times 10^{-2}$			2.699×10^{-2}		
K_s (N/m)	$K_s^0 = \frac{G\pi d_p^4}{32h_p p_b^2} = 1.364 \times 10^2$			2.138×10^2		

The optimization problem is to minimize the sum of squared value of the error that is the difference between the energies at micro- and macro-scale models at every step of loading. The mechanical problem is as follows: Consider a rectangular plate as the macro-scale model representing the pantographic structure at the micro-scale under uni-axial tensile testing. One side is clamped, and the other end is loaded in n equal quasi time steps up to the maximum loading. The stored energy of the structure is calculated after every time step of loading. The objective (error) function is defined as

$$Err(W_M) = \sum_{i=1}^n (W_m^i - W_M^i)^2, \quad (18)$$

where n is the number of steps. Then, the following optimization problem gives the best parameters (K_e, K_g, K_s) being the unknowns for the minimization problem,

$$(K_e, K_g, K_s) = \arg \min_{K_e, K_g, K_s} Err(W_M). \quad (19)$$

The initial guess for the parameters (K_e, K_g, K_s) are calculated as a function of the geometry and material of the pantographic structure, as suggested in [75]. The formulas for the initial guess of the parameters are presented in Table 1, where I_z is the area moment of inertia with regard to z -axis, and G is the shear modulus of the material at the micro-scale. The unknowns are normalized by the values of the initial guess before being set in the optimization code. Therefore, the solution obtained from the optimization will be a factor of the initial guess values, and the parameters are multiplied by the initial guess values before being used in the macro-scale model. The unknown sensitivity of parameters to the error measure is normalized by dividing each parameter to their corresponding initial guess. Hence, the optimization procedure alters them with the same accuracy set by the convergence tolerances.

The employed optimization algorithm, responsible for updating the parameters and distinguishing the path toward the optimum point, is the *Trust Region Reflective* (TRR) algorithm. The TRR algorithm is an improved version of typical trust region algorithms. Trust region methods are well-known as powerful approaches for solving unconstrained nonlinear minimization problems with strong convergence properties. The idea of a trust region method for minimizing a function is as follows. It approximates the objective function, $f(x)$, with a quadratic function, $q(x)$, which simplifies the objective function in a neighborhood, N , around the current point, x . The $q(x)$ is usually formed by the first two terms of the Taylor expansion of $f(x)$ around x . Then, a sub-problem is defined as computing a trial step s and minimizing $q(s)$ within N . After every step, if the cost (objective) function at the point $x + s$ has decreased, the current point is updated to $x + s$, and it is called a successful step. Otherwise, the current point is not changed, but the radius of the region N is reduced for the next step [84].

In TRR, the trust region idea is generalized from unconstrained to bound-constrained nonlinear minimization problem. Using a novel reflection technique, in TRR, the convergence is accelerated, and it features high computational efficiency and robustness. The TRR is based on the interior reflective Newton algorithm, as proposed in [85]. The interior reflective method does the iterations within a confined interior of the feasible region, which is defined by the upper and lower bound constraints of the variables [86].

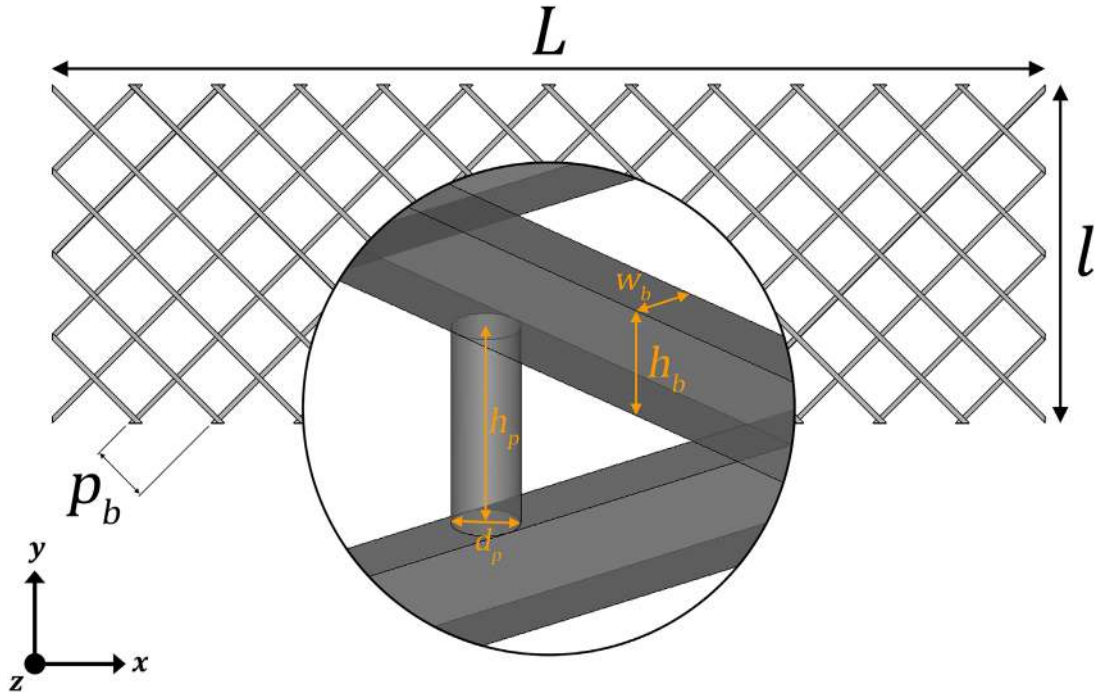


FIGURE 4 The geometrical dimensions depicted on the pantographic structure

After every iteration of the optimization, the numerical solution of macro-scale model is repeated, and the convergence of the optimization problem is assessed through three criteria. For this purpose, I) the reduction (change) of the cost function, II) the norm of the step s , and III) the infinity norm of the scaled gradient of the objective function are calculated and checked by the criteria using the convergence tolerances. The scaled gradient is calculated by accounting for the presence of the parameter bounds. As soon as any of the above-mentioned criteria is satisfied, the optimization loop terminates, and the best constitutive parameters for the macro-scale model are obtained as the output of the problem.

4 | GEOMETRY AND MODELING

In this section, a pantographic structure is considered, and the micro-scale and macro-scale models, i.e., the weak forms in Equation (6) and Equation (16), respectively, are implemented for obtaining the deformation in the structure. First, the geometrical and material properties of the structure are presented; then, the details of implementation of the models are discussed.

4.1 | Geometry

The geometry of the pantographic structure considered here is from [46], where the structure was manufactured and inspected through experimental tests. The material of the structure is Polyamide PA 2200, a polymer modeled as an isotropic, linear elastic material with Young's modulus $E = 1600$ MPa and Poisson's ratio $\nu = 0.3$. The geometrical dimensions of the structure are presented in Figure 4 and Table 1.

4.2 | Modeling and boundary conditions

For building the micro-scale CAD model of the structure as depicted in Figure 1, the open-source SALOME platform [87] is used. The model is meshed with tetrahedral continuum elements using NETGEN algorithm [88], as shown in Figure 5. There are 76449 nodes, meaning around 230k degrees of freedom, in this mesh. For the macro-scale implementation, a

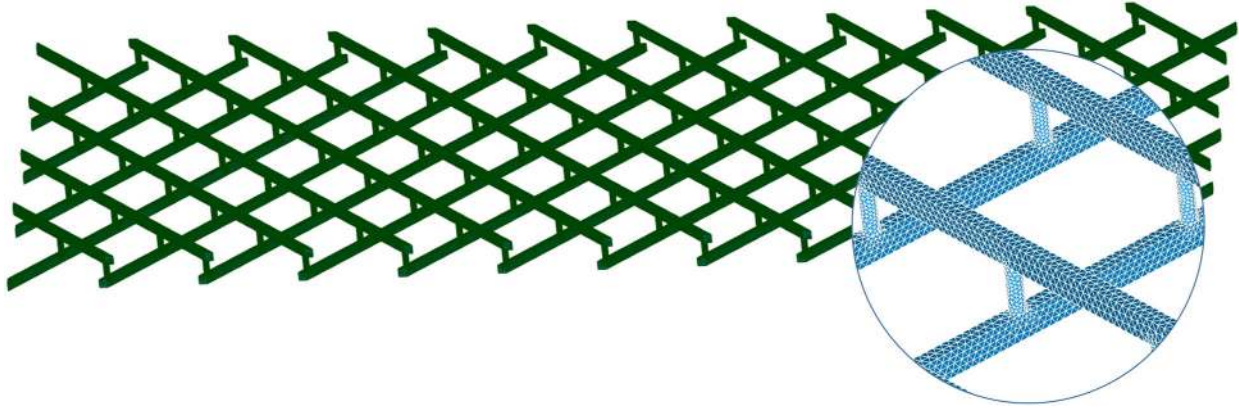


FIGURE 5 The mesh of the pantographic structure

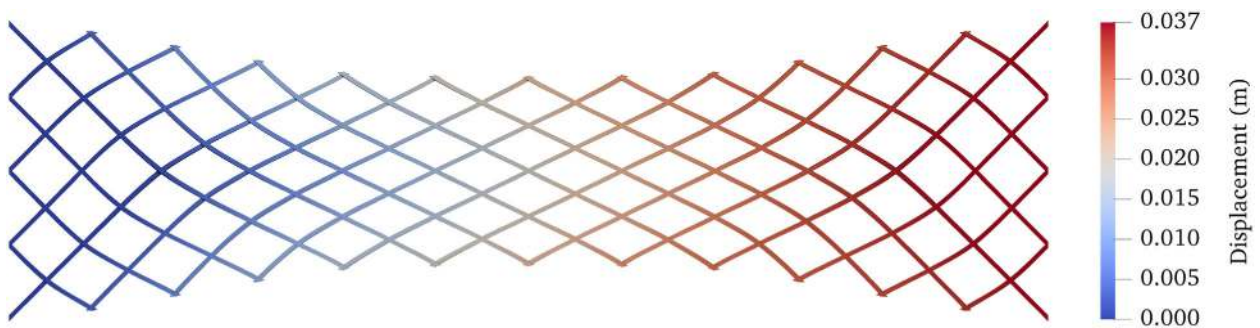


FIGURE 6 Simulation of a tensile test of the pantographic structure by micro-scale modeling (17.6% normal strain, displacement is shown without scaling in ParaView)

two-dimensional (2D) rectangle is created and meshed with triangular elements with around 1300 degrees of freedom. We remark that the computational cost increases exponentially regarding the degrees of freedom.

For a uniaxial tensile test, left and right ends are given by the Dirichlet boundary conditions. For both the 3D and the 2D models, the left side of the structure is clamped, and the right side is moved for 37 mm, applied in eight quasi time steps so that we will obtain the solution at every step of displacement.

4.3 | Numerical implementation

The micro- and macro-scale continuum models discussed in Section 2 are implemented on the respective CAD models. For solving the weak forms of the two models numerically and applying the boundary conditions, the models are implemented into the finite-element code in the FEniCS platform [89], which is an open-source computing platform for automated solution of partial differential equations. The Newton–Raphson method is utilized for linearizing the nonlinear differential equations. For the convergence study of the macro-scale model, see the appendix.

5 | RESULTS AND DISCUSSION

The results of the simulation of a tensile test on the pantographic structure obtained from micro- and macro-scale modelings are presented. The visualizations are done in ParaView [90]. By solving the weak form of the micro-scale model, the deformation of the structure, as the primitive variable of the problem, is obtained. Figure 6 shows the displacement in the pantographic structure for a displacement of 37 mm (17.6% normal strain) in the tensile test.

The same boundary conditions for the tensile test are applied on the homogenized model of the macro-scale model. Through the optimization process, the parameters, K_e , K_g , K_s in Eq. (15) are determined and compiled in Table 1. By setting

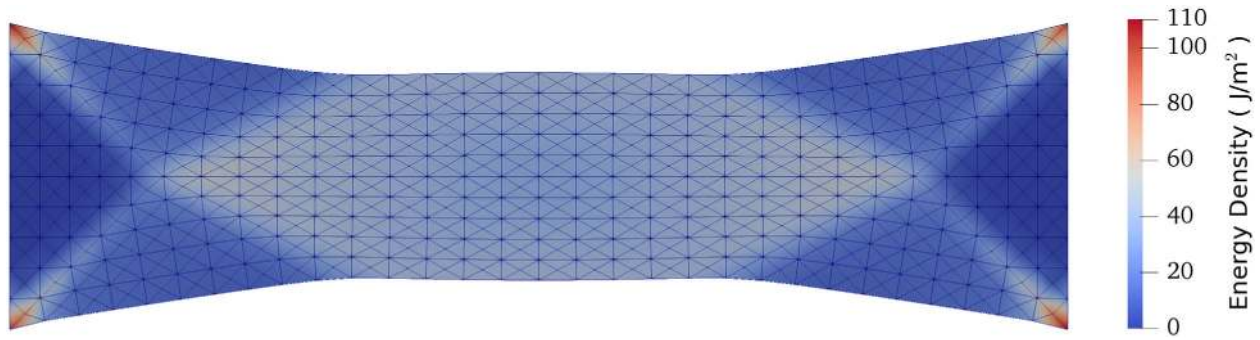


FIGURE 7 Energy density in the tensile test simulated by the macro-scale homogenized model with the used mesh (17.6% normal strain, displacement is presented without scaling, in ParaView)

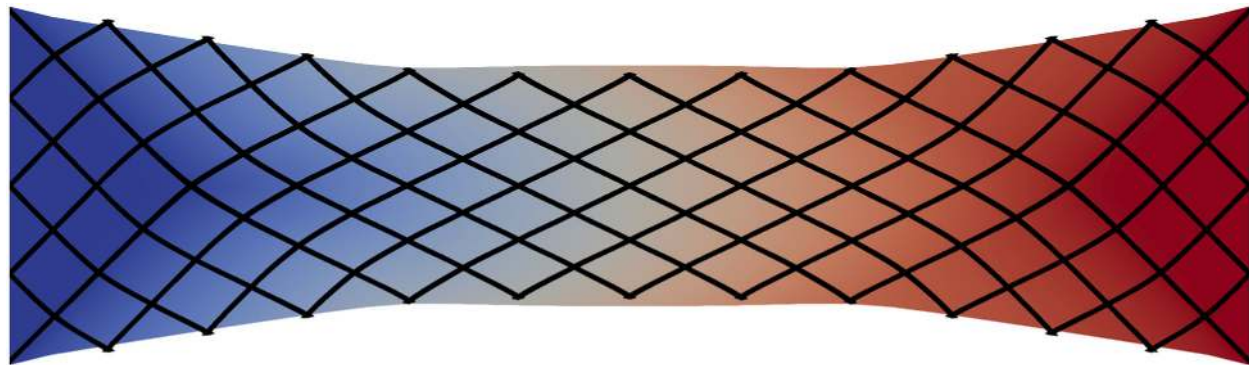


FIGURE 8 Comparison of the deformations by micro- and macro-scale modelings (micro-scale model: in black lines, macro-scale model: in color)

these parameters in the macro-scale model, the deformation and energy density shown in Figure 7 are obtained. In order to compare the consistency of the models, the deformations calculated by the micro- and macro-scale models are plotted on each other in Figure 8.

As shown in Figure 8, the two approaches show very good consistency, and deformation along the boundary is adequate. The values of total stored energy are plotted and compared in Figure 9. As the loading is applied in eight time steps, the energy is calculated at each step. The graph denotes that the optimization algorithm has minimized the error between the energies of macro- and micro-scale models.

FIGURE 9 The values of total stored energy from the macro- and micro-scale models

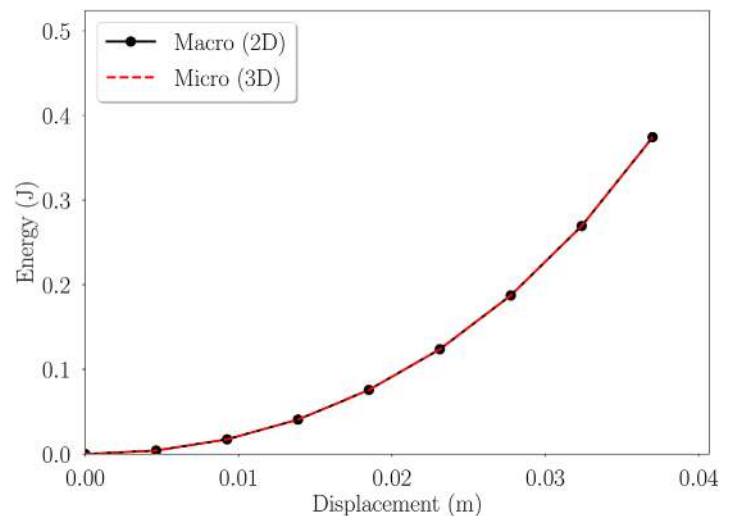
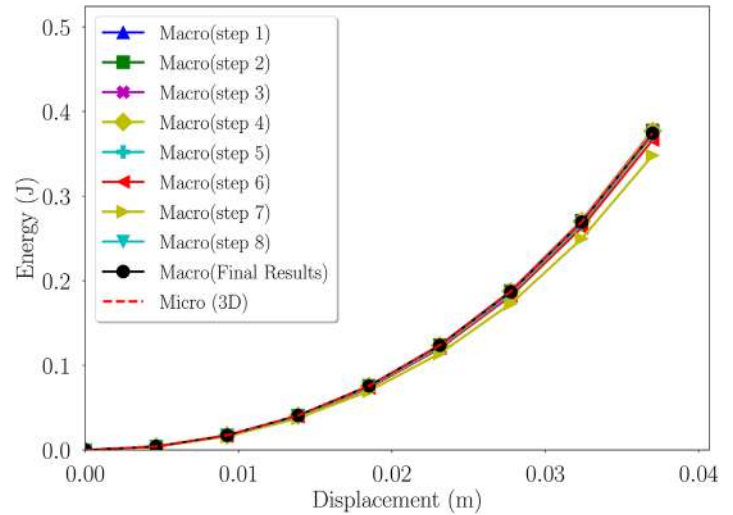


TABLE 2 Sensitivity analysis

Parameter	Displacement (mm)							
	4.6	9.2	13.9	18.5	23.1	27.7	32.4	37.0
K_e/K_e^0	1.011	1.021	1.029	1.042	1.065	1.100	1.094	1.097
K_g/K_g^0	1.026	1.035	1.037	1.036	1.032	1.025	1.018	1.032
K_s/K_s^0	1.550	1.573	1.572	1.568	1.555	1.519	1.440	1.543

FIGURE 10 Energy calculated by using the parameters from the sensitivity study



In order to check the sensitivity of the model, the constitutive parameters are determined after every loading step, as shown in Table 2. The values in Table 2 are given as a factor of the initial guess values. By setting each set of the parameters of Table 2 in the macro-scale model, the energy is calculated and compared in Figure 10. The consistency of the plots in Figure 10 shows the robustness and reliability of the macro-scale model.

The results demonstrate that a reduced-order homogenized model simulates the behavior of a metamaterial with a complex structure which has a detailed substructure, and produces comparable results. The computational cost of the reduced-order model is significantly lower than the detailed three-dimensional model.

6 | CONCLUSION

In this paper, a 3D micro-scale continuum model is implemented on a pantographic structure, and it is solved numerically in the FEniCS platform. On the other hand, a macro-scale homogenized model is employed for modeling the same structure, and the constitutive parameters of this model are identified by developing an automatized process by means of FEM computations and an optimization problem. In this optimization problem, the total stored energies obtained from the two models are compared, and the error is minimized. The optimization algorithm utilized here is the Trust Region Reflective method. The results show that the proposed procedure for parameter determination is robust and proves to be consistent with the micro-scale model. Being the error function defined only in terms of kinematic quantities, the application of this method to experimental model identifications based on full-field kinematic measurements is foreseen.

ACKNOWLEDGMENTS

The work illustrated in this paper is part of N. Shekarchizadeh's thesis for the Ph.D. course in "Mathematical Models for Engineering, Electromagnetism and Nanosciences" at Sapienza University of Rome.

Open access funding enabled and organized by Projekt DEAL.

ORCID

Navid Shekarchizadeh  <https://orcid.org/0000-0002-5750-7801>

Bilen Emek Abali  <https://orcid.org/0000-0002-8735-6071>

Emilio Barchiesi  <https://orcid.org/0000-0002-7296-0671>

Alberto Maria Bersani  <https://orcid.org/0000-0001-8525-7363>

REFERENCES

- [1] Shekarchizadeh, N., Jafari Nedoushan, R., Dastan, T., Hasani, H.: Experimental and numerical study on stiffness and damage of glass/epoxy biaxial weft-knitted reinforced composites. *J. Reinf. Plast. Compos.* 0731684420938446 (2020)
- [2] Shekarchizadeh, N., Abedi, M.M., Jafari Nedoushan, R.: Prediction of elastic behavior of plain weft-knitted composites. *J. Reinf. Plast. Compos.* 35(22), 1613–1622 (2016)
- [3] Fouladi, A., Jafari Nedoushan, R., Hajrasouliha, J., Sheikhzadeh, M., Kim, Y.-M., Na, W.-J., Yu, W.-R.: Control of braid pattern on every side of a braided composite part produced by asymmetrical braiding process. *Appl. Compos. Mater.* 26(2), 479–492 (2019)
- [4] Abghary, M.J., Jafari Nedoushan, R., Hasani, H.: Multi-scale modeling the mechanical properties of biaxial weft knitted fabrics for composite applications. *Appl. Compos. Mater.* 24(4), 863–878 (2017)
- [5] dell’Isola, F., Lekszycki, T., Pawlikowski, M., Grygoruk, R., Greco, L.: Designing a light fabric metamaterial being highly macroscopically tough under directional extension: first experimental evidence. *Z. Angew. Math. Phys.* 66(6), 3473–3498 (2015)
- [6] Yang, H., Ganzosch, G., Giorgio, I., Abali Bilen, E.: Material characterization and computations of a polymeric metamaterial with a pantographic substructure. *Z. Angew. Math. Phys.* 69(4), 105 (2018)
- [7] Truesdell, C., Noll, W.: The non-linear field theories of mechanics. In: Antman, S.S. (ed.) *The Non-Linear Field Theories of Mechanics*. Springer, Berlin, Heidelberg (2004)
- [8] Altenbach, H., Müller, W.H., Abali, B.E. (eds.): *Higher Gradient Materials and Related Generalized Continua*, Vol. 120 of *Advanced Structured Materials*. Springer, Cham (2019)
- [9] Eremeyev, V.A., Lebedev, L.P., Altenbach, H.: *Foundations of Micropolar Mechanics*. Springer Science & Business Media (2012)
- [10] Abali, B.E., Giorgio, I. (eds.): *Developments and Novel Approaches in Biomechanics and Metamaterials*, Vol. 132 of *Advanced Structured Materials*. Springer, Cham (2020)
- [11] Müller, W.H.: The experimental evidence for higher gradient theories. In: Bertram, A., Forest, S. (eds.) *Mechanics of Strain Gradient Materials*, Vol. 600 of *CISM International Centre for Mechanical Sciences (Courses and Lectures)*, pp. 1–18. Springer, Cham (2020)
- [12] Müller, W.H., Vilchevskaya, E.N.: Micropolar theory with production of rotational inertia: a rational mechanics approach. In: Altenbach, H., Pouget, J., Rousseau, M., Collet, T. (eds.) *Generalized Models and Non-classical Approaches in Complex Materials 1*, Vol. 89 of *Advanced Structured Materials*, pp. 581–606. Springer, Cham (2018)
- [13] Abali, B.E.: Revealing the physical insight of a length scale parameter in metamaterials by exploring the variational formulation. *Continuum Mech. Thermodyn.* 31(4), 885–894 (2018)
- [14] Abali, B.E., Müller, W.H., Eremeyev, V.A.: Strain gradient elasticity with geometric nonlinearities and its computational evaluation. *Mechan. Adv. Mater. Modern Processes* 1(1), 1–11 (2015)
- [15] Mindlin, R.D.: *Microstructure in Linear Elasticity*, Department of Civil Engineering and Engineering Mechanics, Columbia University, New York (1963)
- [16] Mindlin, R.D.: Second gradient of strain and surface-tension in linear elasticity. *Int. J. Solids Struct.* 1(4), 417–438 (1965)
- [17] Lazar, M., Maugin, G.A., Aifantis, E.C.: Dislocations in second strain gradient elasticity. *Int. J. Solids Struct.* 43(6), 1787–1817 (2006)
- [18] Mousavi, S.M., Paavola, J.: Analysis of plate in second strain gradient elasticity. *Arch. Appl. Mech.* 84(8), 1135–1143 (2014)
- [19] Aifantis, E.C.: On the microstructural origin of certain inelastic models. *J. Eng. Mater. Technol.* 106(4), 326–330 (1984)
- [20] Fleck, N.A., Muller, G.M., Ashby Mike, F., Hutchinson John, W.: Strain gradient plasticity: theory and experiment. *Acta Metall. Mater.* 42(2), 475–487 (1994)
- [21] Hutchinson, J.W., Fleck, N.: Strain gradient plasticity. *Adv. Appl. Mech.* 33, 295–361 (1997)
- [22] Gao, H., Huang, Y., Nix, W.D., Hutchinson, J.W.: Mechanism-based strain gradient plasticity—I. Theory. *J. Mech. Phys. Solids* 47(6), 1239–1263 (1999)
- [23] Klusemann, B., Kochmann, D.M.: Microstructural pattern formation in finite-deformation single-slip crystal plasticity under cyclic loading: relaxation vs. gradient plasticity. *Comput. Methods Appl. Mech. Eng.* 278, 765–793 (2014)
- [24] Auffray, N., Dirrenberger, J., Rosi, G.: A complete description of bi-dimensional anisotropic strain-gradient elasticity. *Int. J. Solids Struct.* 69, 195–206 (2015)
- [25] Forest, S., Aifantis, E.C.: Some links between recent gradient thermo-elasto-plasticity theories and the thermomechanics of generalized continua. *Int. J. Solids Struct.* 47(25–26), 3367–3376 (2010)
- [26] Bersani, A.M., Caressa, P.: Lagrangian descriptions of dissipative systems: a review. *Math. Mechan. Solids* 1081286520971834 (2020)
- [27] Reda, H., Rahali, Y., Ganghoffer, J.F., Lakiss, H.: Wave propagation analysis in 2D nonlinear hexagonal periodic networks based on second order gradient nonlinear constitutive models. *Int. J. Non Linear Mech.* 87, 85–96 (2016)
- [28] Kouznetsova, V., Geers, M.G.D., Brekelmans, W.A.M.: Multi-scale constitutive modelling of heterogeneous materials with a gradient-enhanced computational homogenization scheme. *Int. J. Numer. Methods Eng.* 54(8), 1235–1260 (2002)

- [29] Geers, M.G.D., Kouznetsova, V., Brekelmans, W.A.M.: Gradient-enhanced computational homogenization for the micro-macro scale transition. *Le Journal de Physique IV* 11(PR5), Pr5–145 (2001)
- [30] Barboura, S., Li, J.: Establishment of strain gradient constitutive relations by using asymptotic analysis and the finite element method for complex periodic microstructures. *Int. J. Solids Struct.* 136, 60–76 (2018)
- [31] Neff, P., Ghiba, I.-D., Madeo, A., Placidi, L., Rosi, G.: A unifying perspective: the relaxed linear micromorphic continuum. *Continuum Mech. Thermodyn.* 26(5), 639–681 (2014)
- [32] Niiranen, J., Kiendl, J., Niemi Antti, H., Reali, A.: Isogeometric analysis for sixth-order boundary value problems of gradient-elastic Kirchhoff plates. *Comput. Methods Appl. Mech. Eng.* 316, 328–348 (2017)
- [33] Mousavi, S.M., Reddy, J.N., Romanoff, J.: Analysis of anisotropic gradient elastic shear deformable plates. *Acta Mech.* 227(12), 3639–3656 (2016)
- [34] Balabanov, V., Niiranen, J.: Locking-free variational formulations and isogeometric analysis for the Timoshenko beam models of strain gradient and classical elasticity. *Comput. Methods Appl. Mech. Eng.* 339, 137–159 (2018)
- [35] Madeo, A., George, D., Lekszycki, T., Nierenberger, M., Rémond, Y.: A second gradient continuum model accounting for some effects of micro-structure on reconstructed bone remodelling. *C.R. Math.* 340(8), 575–589 (2012)
- [36] Cuomo, M., dell’Isola, F., Greco, L.: Simplified analysis of a generalized bias test for fabrics with two families of inextensible fibres: *Z. Angew. Math. Phys.* 67(3), 61 (2016)
- [37] dell’Isola, F., Cuomo, M., Greco, L., Della Corte, A.: Bias extension test for pantographic sheets: numerical simulations based on second gradient shear energies. *Int. J. Eng. Math.* 103(1), 127–157 (2017)
- [38] dell’Isola, F., Della Corte, A., Greco, L., Luongo, A.: Plane bias extension test for a continuum with two inextensible families of fibers: a variational treatment with Lagrange multipliers and a perturbation solution. *Int. J. Solids Struct.* 81, 1–12 (2016)
- [39] Placidi, L., Greco, L., Bucci, S., Turco, E., Rizzi, N.L.: A second gradient formulation for a 2D fabric sheet with inextensible fibres. *Z. Angew. Math. Phys.* 67(5), 114 (2016)
- [40] Greco, L., Giorgio, I., Battista, A.: In plane shear and bending for first gradient inextensible pantographic sheets: numerical study of deformed shapes and global constraint reactions. *Math. Mechan. Solids* 22(10), 1950–1975 (2017)
- [41] Challamel, N., Kocsis, A., Wang, C.M.: Discrete and non-local elastica: *Int. J. Non Linear Mech.* 77, 128–140 (2015)
- [42] Turco, E., dell’Isola, F., Cazzani, A., Rizzi, N.L.: Hencky-type discrete model for pantographic structures: numerical comparison with second gradient continuum models. *Z. Angew. Math. Phys.* 67(4), 85 (2016)
- [43] Turco, E., Giorgio, I., Misra, A., dell’Isola, F.: King post truss as a motif for internal structure of (meta) material with controlled elastic properties. *R. Soc. Open Sci.* 4(10), 171153 (2017)
- [44] Barchiesi, E., Khakalo, S.: Variational asymptotic homogenization of beam-like square lattice structures. *Math. Mechan. Solids* 24(10), 3295–3318 (2019)
- [45] Turco, E., Barchiesi, E., Giorgio, I., dell’Isola, F.: A Lagrangian Hencky-type non-linear model suitable for metamaterials design of shearable and extensible slender deformable bodies alternative to Timoshenko theory. *Int. J. Non Linear Mech.* 103481 (2020)
- [46] Andreaus, U., Spagnuolo, M., Lekszycki, T., Eugster, S.R.: A Ritz approach for the static analysis of planar pantographic structures modeled with nonlinear Euler–Bernoulli beams. *Continuum Mech. Thermodyn.* 30(5), 1103–1123 (2018)
- [47] dell’Isola, F., Della Corte, A., Giorgio, I., Scerrato, D.: Pantographic 2D sheets: discussion of some numerical investigations and potential applications. *Int. J. Non Linear Mech.* 80, 200–208 (2016)
- [48] Harrison, P.: Modelling the forming mechanics of engineering fabrics using a mutually constrained pantographic beam and membrane mesh. *Composites, Part A* 81, 145–157 (2016)
- [49] Alibert, J.-J., Seppecher, P., dell’Isola, F.: Truss modular beams with deformation energy depending on higher displacement gradients. *Math. Mechan. Solids* 8(1), 51–73 (2003)
- [50] Rahali, Y., Ganghoffer, J.-F., Chaouachi, F., Zghal, A.: Strain gradient continuum models for linear pantographic structures: a classification based on material symmetries. *J. Geometry Symmetry Physics* 40, 35–52 (2015)
- [51] Scerrato, D., Zhurba Eremeeva, I.A., Lekszycki, T., Rizzi, N.L.: On the effect of shear stiffness on the plane deformation of linear second gradient pantographic sheets. *J. Appl. Math. Mech.* 96(11), 1268–1279 (2016)
- [52] Steigmann, D.J., dell’Isola, F.: Mechanical response of fabric sheets to three-dimensional bending, twisting, and stretching. *Acta Mech. Sin.* 31(3), 373–382 (2015)
- [53] Barchiesi, E., Eugster, S.R., Placidi, L., dell’Isola, F.: Pantographic beam: a complete second gradient 1D-continuum in plane. *Z. Angew. Math. Phys.* 70(5), 135 (2019)
- [54] Turco, E., Misra, A., Pawlikowski, M., dell’Isola, F., Hild, F.: Enhanced Piola–Hencky discrete models for pantographic sheets with pivots without deformation energy: numerics and experiments: *Int. J. Solids Struct.* 147, 94–109 (2018)
- [55] Placidi, L., Andreaus, U., Giorgio, I.: Identification of two-dimensional pantographic structure via a linear D4 orthotropic second gradient elastic model. *Int. J. Eng. Math.* 103(1), 1–21 (2017)
- [56] dell’Isola, F., Seppecher, P., Spagnuolo, M., Barchiesi, E., Hild, F., Lekszycki, T., Giorgio, I., Placidi, L., Andreaus, U., Cuomo, M., Eugster, S.R., Pfaff, A., Hoschke, K., Langkemper, R., Turco, E., Sarikaya, R., Misra, A., De Angelo, M., D’Annibale, F., Bouterf, A., Pinelli, X., Misra, A., Desmorat, B., Pawlikowski, M., Dupuy, C., Scerrato, D., Peyre, P., Laudato, M., Manzari, L., Göransson, P., Hesch, C., Hesch, S., Franciosi, P., Dirrenberger, J., Maurin, F., Vangelatos, Z., Grigoropoulos, C., Melissinaki, V., Farsari, M., Muller, W., Emek Abali, B., Liebold, C., Ganzosch, G., Harrison, P., Drobnicki, R., Igumnov, L., Alzahrani, F., Hayat, T.: Advances in pantographic structures: design, manufacturing, models, experiments and image analyses. *Continuum Mech. Thermodyn.* 31(4), 1231–1282 (2019)

- [57] dell'Isola, F., Seppecher, P., Alibert, J.J., Lekszycki, T., Grygoruk, R., Pawlikowski, M., Steigmann, D., Giorgio, I., Andreaus, U., Turco, E., Golaszewski, M., Rizzi, N., Boutin, C., Eremeyev, V.A., Misra, A., Placidi, L., Barchiesi, E., Greco, L., Cuomo, M., Cazzani, A., Della Corte, A., Battista, A., Scerrato, D., Zurba Eremeeva, I., Rahali, Y., Ganghoffer, J.-F., Müller, W., Ganzosch, G., Spagnuolo, M., Pfaff, A., Barcz, K., Hoschke, K., Neggers, J., Hild, F.: Pantographic metamaterials: an example of mathematically driven design and of its technological challenges. *Continuum Mech. Thermodyn.* 31(4), 851–884 (2019)
- [58] Yildizdag, M.E., Barchiesi, E., dell'Isola, F.: Three-point bending test of pantographic blocks: numerical and experimental investigation. *Math. Mech. Solids* 25(10), 1965–1978 (2020)
- [59] Turco, E., Barchiesi, E.: Equilibrium paths of Hencky pantographic beams in a three-point bending problem. *Math. Mech. Complex Syst.* 7(4), 287–310 (2019)
- [60] Mandadapu, K.K., Abali, B.E., Papadopoulos, P.: On the polar nature and invariance properties of a thermomechanical theory for continuum-on-continuum homogenization. *arXiv preprint arXiv:1808.02540* (2018)
- [61] Yang, H., Abali, B.E., Timofeev, D., Müller Wolfgang, H.: Determination of metamaterial parameters by means of a homogenization approach based on asymptotic analysis. *Continuum Mech. Thermodyn.* 1–20 (2019)
- [62] Abali, B.E., Yang, H., Papadopoulos, P.: A computational approach for determination of parameters in generalized mechanics. In: Altenbach, H., Müller, W.H., Abali, B.E. (eds.) *Higher Gradient Materials and Related Generalized Continua*, Vol. 120 of *Advanced Structured Materials*, pp. 1–18. Springer, Cham (2019)
- [63] Eremeyev, V.A., dell'Isola, F., Boutin, C., Steigmann, D.: Linear pantographic sheets: existence and uniqueness of weak solutions. *J. Elast.* 132(2), 175–196 (2018)
- [64] Eremeyev, V.A., dell'Isola, F.: Weak solutions within the gradient-incomplete strain-gradient elasticity. *Lobachevskii J. Math.* 41(10), 191–197 (2020)
- [65] Barchiesi, E., Laudato, M., Di Cosmo, F.: Wave dispersion in non-linear pantographic beams. *Mech. Res. Commun.* 94, 128–132 (2018)
- [66] Laudato, M., Manzari, L.: Linear dynamics of 2D pantographic metamaterials: numerical and experimental study. In: *Developments and Novel Approaches in Biomechanics and Metamaterials*, pp. 353–375. Springer (2020)
- [67] Laudato, M., Manzari, L., Barchiesi, E., Di Cosmo, F., Göransson, P.: First experimental observation of the dynamical behavior of a pantographic metamaterial. *Mech. Res. Commun.* 94, 125–127 (2018)
- [68] Tran, C.A., Gołaszewski, M., Barchiesi, E.: Symmetric-in-plane compression of polyamide pantographic fabrics—modelling, experiments and numerical exploration. *Symmetry* 12(5), 693 (2020)
- [69] Barchiesi, E., Eugster, S.R., dell'Isola, F., Hild, F.: Large in-plane elastic deformations of bi-pantographic fabrics: asymptotic homogenization and experimental validation. *Math. Mech. Solids* 25(3), 739–767 (2020)
- [70] Eremeyev, V.A., Ganghoffer, J.-F., Konopińska-Zmysłowska, V., Uglov Nikolay, S.: Flexoelectricity and apparent piezoelectricity of a pantographic micro-bar. *Int. J. Eng. Sci.* 149, 103213 (2020)
- [71] Mawassy, N., Reda, H., Ganghoffer, J.-F., Eremeyev, V.A., Lakiss, H.: A variational approach of homogenization of piezoelectric composites towards piezoelectric and flexoelectric effective media. *Int. J. Eng. Sci.* 158, 103410 (2021)
- [72] dell'Isola, F., Giorgio, I., Pawlikowski, M., Rizzi, N.L.: Large deformations of planar extensible beams and pantographic lattices: heuristic homogenization, experimental and numerical examples of equilibrium. *Proc. R. Soc. A: Math. Phys. Eng. Sci.* 472(2185), 20150790 (2016)
- [73] Giorgio, I., Rizzi, N.L., Turco, E.: Continuum modelling of pantographic sheets for out-of-plane bifurcation and vibrational analysis. *Proc. R. Soc. A: Math. Phys. Eng. Sci.* 473(2207), 20170636 (2017)
- [74] Giorgio, I.: Numerical identification procedure between a micro-Cauchy model and a macro-second gradient model for planar pantographic structures. *Z. Angew. Math. Phys.* 67(4), 95 (2016)
- [75] De Angelo, M., Barchiesi, E., Giorgio, I., Abali, B.E.: Numerical identification of constitutive parameters in reduced-order bi-dimensional models for pantographic structures: application to out-of-plane buckling. *Arch. Appl. Mechan.* 89(7), 1333–1358 (2019)
- [76] Shekarchizadeh, N., Abedi, M.: Determining the constitutive parameters of a macro-scale second-gradient Model for planar pantographic structures by using optimization algorithms. *Proceedings of 8th GACM Colloquium on Computational Mechanics: For Young Scientists From Academia and Industry*, pp. 31–34 (2019)
- [77] Abraham, A., Jain, L.: Evolutionary multiobjective optimization. In: Abraham, A., Jain, L., Goldberg, R. (eds.) *Evolutionary Multiobjective Optimization*, of *Advanced Information and Knowledge Processing*, pp. 1–6. Springer, London (2005)
- [78] Deb, K., Pratap, A., Agarwal, S., Meyarivan, T.: A fast and elitist multiobjective genetic algorithm: NSGA-II. *IEEE Trans. Evol. Comput.* 6(2), 182–197 (2002)
- [79] Abali, B.E.: *Computational Reality*, Vol. 55, *Advanced Structured Materials*. Springer Nature, Singapore (2017)
- [80] Abali, B.E., Müller, W.H.: Numerical solution of generalized mechanics based on a variational formulation. *Oberwolfach Rep. - Mechan. Mater.* 17(1), 9–12 (2016)
- [81] Giorgio, I., Della Corte, A., dell'Isola, F., Steigmann, D.J.: Buckling modes in pantographic lattices. *C.R. Mec.* 344(7), 487–501 (2016)
- [82] Bersani, A.M., dell'Isola, F., Seppecher, P.: Lagrange multipliers in infinite dimensional spaces, examples of application. In: Altenbach, H., Öchsner, A. (eds.) *Encyclopedia of Continuum Mechanics*, pp. 1–8. Springer, Berlin, Heidelberg (2019)
- [83] Virtanen, P., Gommers, R., Oliphant, T.E., Haberland, M., Reddy, T., Cournapeau, D., Burovski, E., Peterson, P., Weckesser, W., Bright, J., van der Walt, S.J., Brett, M., Wilson, J., Jarrod Millman, K., Mayorov, N., Nelson, A.R.J., Jones, E., Kern, R., Larson, E., Carey, C.J., Polat, I., Feng, Y., Moore, E.W., VanderPlas, J., Laxalde, D., Perktold, J., Cimrman, R., Henriksen, I., Quintero, E.A., Harris, C.R., Archibald, A.M., Ribeiro, A.H., Pedregosa, F., van Mulbregt, P., SciPy 1.0 Contributors: SciPy 1.0: Fundamental algorithms for scientific computing in Python. *Nat. Methods* 17, 261–272 (2020)

- [84] Le, T.M., Fatahi, B., Khabbaz, H., Sun, W.: Numerical optimization applying trust-region reflective least squares algorithm with constraints to optimize the non-linear creep parameters of soft soil. *Appl. Math. Modell.* 41, 236–256 (2017)
- [85] Coleman, T.F., Li, Y.: An interior trust region approach for nonlinear minimization subject to bounds. *SIAM J. Optim.* 6(2), 418–445 (1996)
- [86] Branch, M.A., Coleman, T.F., Li, Y.: A subspace, interior, and conjugate gradient method for large-scale bound-constrained minimization problems. *SIAM J. Scientific Computing* 21(1), 1–23 (1999)
- [87] Ribes, A., Caremoli, C.: Salome platform component model for numerical simulation. In: 31st Annual International Computer Software and Applications Conference (COMPSAC 2007), pp. 553–564. IEEE (2007)
- [88] Schöberl, J.: NETGEN An advancing front 2D/3D-mesh generator based on abstract rules. *Computing Visual. Sci.* 1(1), 41–52 (1997)
- [89] Logg, A., Mardal, K.-A., Wells, G.N. (eds): *Automated Solution of Differential Equations by the Finite Element Method*. Springer, Cham (2012)
- [90] Ahrens, J., Geveci, B., Law, C.: ParaView: an end-user tool for large data visualization. *The Visualization Handbook*, p. 717 (2005)

How to cite this article: Shekarchizadeh N, Abali BE, Barchiesi E, Bersani AM. Inverse analysis of metamaterials and parameter determination by means of an automatized optimization problem. *Z Angew Math Mech.* 2021;e202000277. <https://doi.org/10.1002/zamm.202000277>

APPENDIX

The convergence of the macro-scale model is discussed here. Monotonous convergence is achieved as expected from the finite element method. The mesh size is checked by using h -convergence. As in Figure A.1, the h -convergence shows a linear relation in the log-log scale. The h -convergence results are compiled in Table A.1 with *a posteriori* error analysis.

FIGURE A.1 Mesh convergence of the macro-scale model: Energy versus the number of nodes in log-log scale

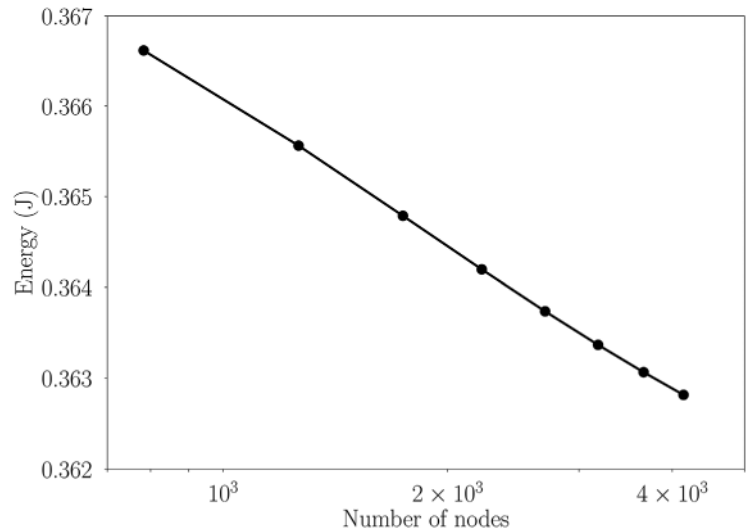


TABLE A.1 Convergence results

	Number of nodes							
	783	1097	1469	1899	2379	2909	3497	4143
Energy (J)	0.3666	0.3655	0.3647	0.3641	0.3637	0.3633	0.3630	0.3628
Error (%)		0.29	0.21	0.16	0.13	0.10	0.08	0.07